ATATÜRK ÜNİVERSİTESİ YAYINLARI
ATATURK UNIVERSITY PUBLICATIONS

NanoEra

Research Article

DOI: 10.5152/NanoEra.2023.23009

Nano-Clean: Titanium Dioxide Nanoparticles Via Sol–Gel for Effective Pollutant Removal

Bachir YAOU BALARABE[1]
Irédon ADJAMA[2]
Moumouni Wagé ABDOUL RAZAK[3]
Hassimi MOUSSA[4]
Abdoul Bari IDI AWALI[5]
Maman Nasser ILLIASSOU OUMAROU[2]

[1]School of Engineering and Technology, National Forensic Sciences University, Gandhinagar, India
[2]School of Pharmacy, National Forensic Sciences University, Gandhinagar, India
[3]Department of Exact Sciences, University Andre Salifou, Faculty of Science and Technology, Zinder, Niger
[4]Department of Environmental Sciences, Boubakar Ba University of Tillaberi, Faculty of Agronomic Sciences, Tillaberi, Niger
[5]Department of Chemistry, Abdou Moumouni University, Faculty of Science and Technology, Niamey, Niger

Received: 11.09.2023
Accepted: 21.12.2023
Publication Date: 31.12.2023

Corresponding author:
Bachir YAOU BALARABE
E-mail: bachir.phdnt21@nfsu.ac.in

Cite this article as: Yaou Balarabe B, Adjama I, Wagé Abdoul Razak M, Moussa H, Bari Idi Awali A, Nasser Illiassou Oumarou M. Nano-clean: TiO_2 nanoparticles via sol-gel for effective pollutant removal. *NanoEra* 2023;3(2):61-66.

ABSTRACT

The research focused on the hydrothermal synthesis of titanium dioxide (TiO_2) nanoparticles, with a detailed analysis of their chemical attributes through Fourier transform infrared and ultraviolet–visible diffuse reflectance spectroscopy, emphasizing the optical features. The nanoparticles' high purity was further affirmed by energy-dispersive X-ray analysis. Transmission electron microscopy revealed spherical particles measuring ≥80 nm. Furthermore, X-ray diffraction and Raman analyses show the anatase structure of the nanomaterial. Under exposure to ultraviolet light, the photocatalytic assessment of 100 mg of the as-synthesized TiO_2 nanoparticles exhibited an impressive efficiency of 77%-90%, successfully removing 30 ppm each of rhodamine B, nonylphenol, roxarsone, and ciprofloxacin within a 105-minute timeframe.

Keywords: Nanoparticles, Pollutant, Removal, TiO2, UV light

INTRODUCTION

Industrial wastewater discharges, especially from the textile industry, constitute a significant source of environmental pollution and pose a serious threat to life on Earth.[1-4] In addition to textile effluents, nonylphenol, an endocrine disruptor and a toxic intermediate degradation product of nonylphenol ethoxylates surfactants, poses a significant threat to the environment.[5,6] The presence of antibiotics in various aquatic environments, including surface water, groundwater, and sewage treatment plant effluents, indicates another emerging environmental problem.[7-9] Roxarsone, a commonly used animal feed additive, is excreted into fertilizer without modifications.[10,11] This fertilizer, frequently used on soil, releases significant quantities of roxarsone, an antimicrobial agent, into the surrounding environment.[12,13] In addition to the contamination of groundwater and surface water, these pollutants possess the capacity to potentially compromise water bodies through the processes of leaching and runoff.[14-16] To address this risk, the timely removal of pollutants from contaminated wastewater is imperative. Commonly utilized methods for pollution remediation include adsorption, coagulation, membrane filtration, and sedimentation.[17] While these technologies have proven to be effective, the target pollutant is often transferred from one medium to another rather than being completely eliminated.[18] To effectively manage sludge or waste streams, secondary processes are necessary. One potential solution is the utilization of advanced oxidation processes. These processes generate highly oxidizing free radicals capable of mineralizing organic compounds, thereby preventing the formation of waste products.[7,19] Advanced oxidation processes have garnered considerable attention for their economic viability at a commercial scale. Due to its affordability, chemical stability, and high efficiency in degrading pollutants when exposed to ultraviolet (UV) light, titanium oxide has become the preferred photocatalyst.[20] Titanium dioxide has 3 natural polymorphs: anatase, rutile, and brookite. Both anatase and rutile share a tetragonal crystal structure due to their chemical stability. Brookite, less common, possesses an orthorhombic crystal structure. In the remediation of organic pollutants, these variations in crystal structure and particle morphology play a crucial role in influencing the photocatalytic effectiveness of semiconductor catalysts.[21] In this study, we assess the photocatalytic efficiency of anatase-phase TiO_2 in degrading 4 distinct pollutants.[22] Providing precise control over material properties and reducing hydrolysis, sol–gel synthesis is considered ideal for tailored materials. However, its appropriateness relies on the specific material and the desired characteristics.[23-25] Using heterogeneous TiO_2 photocatalysis, we discuss the non-aqueous synthesis of TiO_2 nanoparticles for the removal of 4 persistent pollutants, including roxarsone, nonylphenol, rhodamine B, and ciprofloxacin from aquatic systems.

MATERIAL AND METHODS

Materials

Analysis of the sample involved employing various spectroscopic and analytical techniques. The JASCO-670 UV/visible (Vis)/near-infrared (IR) spectroscopy captured optical absorbance spectra, while Fourier transform (FT) IR spectra were recorded with the FT-4700 spectroscopy. Transmission electron microscopy (TEM) images were obtained using a Talos F200i S/TEM electron microscope (HRTEM-200KV). Raman spectra were recorded via Invia Raman spectroscopy, and X-ray diffraction (XRD) patterns were acquired with GNR APD 2000 PRO's Cu-K light source. X-ray photoelectron spectra (XPS) were meticulously measured utilizing a Thermo Scientific K-Alpha instrument with an Al Kα radiation source.

For the synthesis of sol–gel anatase TiO_2 and the assessment of the nanomaterial's removal potential, reagents were procured from Sigma–Aldrich. These included ethanol ([High-performance liquid chromatography] HPLC gradient grade, 99.9%), titanium (IV) butoxide (reagent grade, 97%), and acetic acid (glacial, ≥99%). Figure 1 illustrates the chemical structures obtained from Sigma–Aldrich for the 4 persistent contaminants used in the study, each indicating its respective purity: nonylphenol (99% purity), roxarsone (98% purity), ciprofloxacin (98.0% purity), and rhodamine B (95% purity).

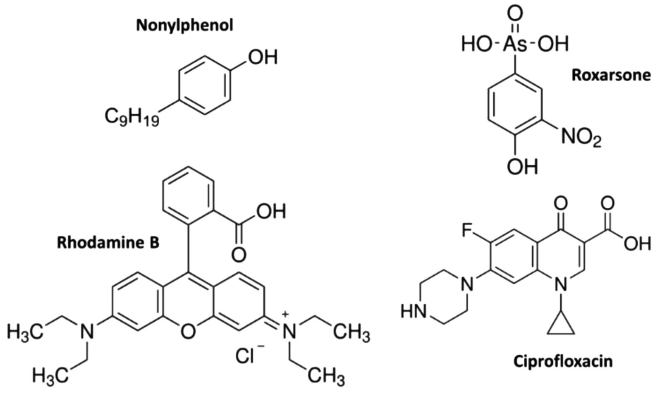

Figure 1. Chemical structure of the pollutants used for the study.

Methods

Synthesis of Titanium Dioxide Nanoparticles

The synthesis of TiO_2 nanoparticles followed a procedure derived from our previous method.[26] In summary, 30 mL of ethanol were mixed with 20 mL of titanium butoxide and 10 mL of acetic acid. The mixture underwent stirring for 15 hours to facilitate the proper formation of nanoparticles. Subsequently, the resulting gel was matured at 80°C for 9 hours, followed by a 3-hour calcination process at 450°C to produce the nanoparticles. After completing the calcination, the particles were collected and subjected to multiple ethanol washes to eliminate impurities, and finally air-dried at room temperature.

Photocatalytic Activity Measurements

The photocatalytic experiment mirrors our previous research (referenced as Figure 2). Employing a photocatalytic reactor paired with a 125-watt high-pressure mercury UV light source operating at room temperature, we aimed to remove nonylphenol, roxarsone, rhodamine B, and ciprofloxacin in the presence of TiO_2 nanoparticles. In a reactor containing 250 mL of an aqueous solution, each pollutant was present at 30 ppm along with 100 mg of TiO_2 nanoparticles for the photodegradation process.

Before exposing the mixture to irradiation, the stirring process lasted for 20 minutes in the dark using a magnetic stirrer to establish adsorption–desorption equilibrium. Throughout the photoreaction process, the absorbance of 1 mL of solution was measured at regular intervals using a UV-Vis spectrometer. As the concentration of the target substance decreased over time, the absorbance peak also decreased, indicating a reduction in pollutant concentration.

Equation 1, presented below, is typically used to calculate the degradation efficiency of the photocatalyst:

$$\textit{Degradation efficiency}\ (\%) = \frac{\mathbf{Conc.}_0 - \mathbf{Conc.}_t}{\mathbf{Conc.}_0} \times 100 \qquad (1)$$

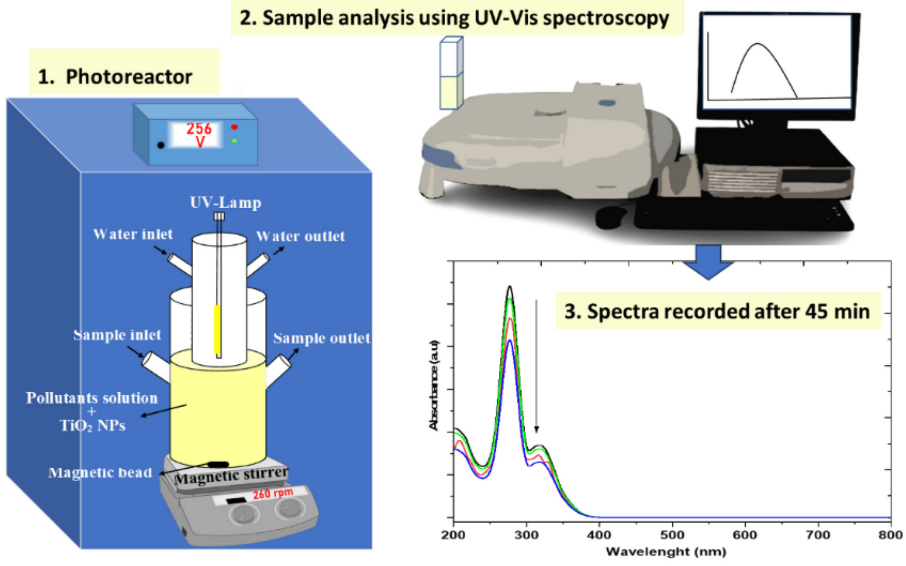

Figure 2. Photocatalytic experiment. UV-Vis, ultraviolet–visible.

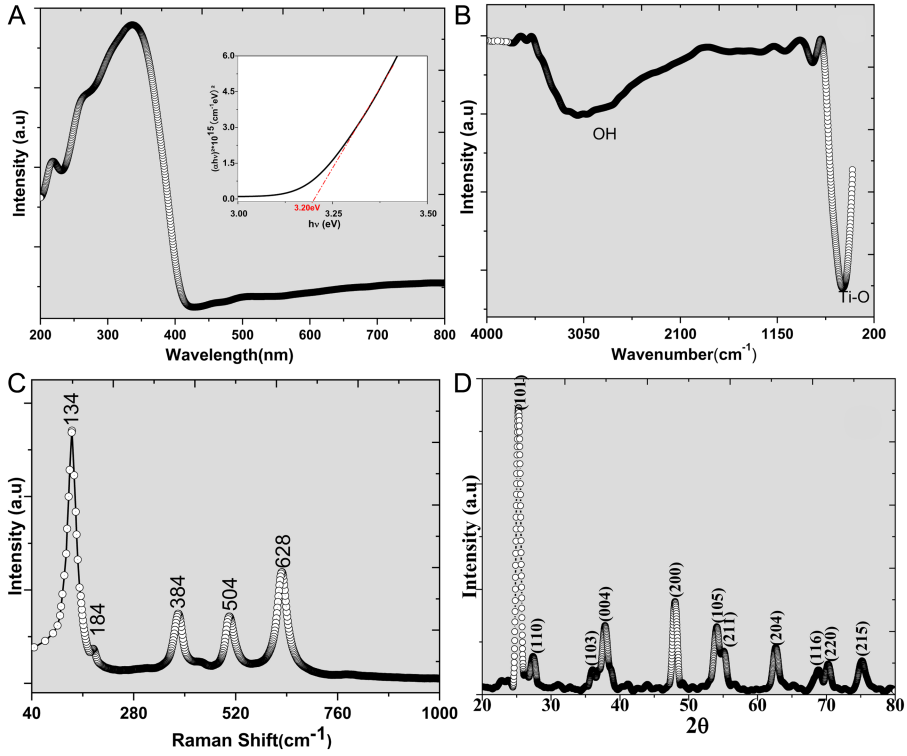

Figure 3. A) Ultraviolet–visible diffuse reflectance spectra, B) the calculated bandgap, C) Raman, and D) X-ray diffraction spectra of TiO_2 nanoparticles.

The variable **Conc.**$_0$ signifies the initial concentration of the specific pollutant present at equilibrium before the commencement of the experiment. On the other hand, **Conc.**$_t$ represents the concentration of the said pollutant that remains after a duration of *t* during the photocatalytic degradation process.[27-29]

RESULTS AND DISCUSSION

Within the 200-400 nm range, the characteristics of absorption peaks of TiO_2 nanoparticles are illustrated in Figure 3A, with the primary peak recorded at 350 nm. The inset of Figure 2A reveals

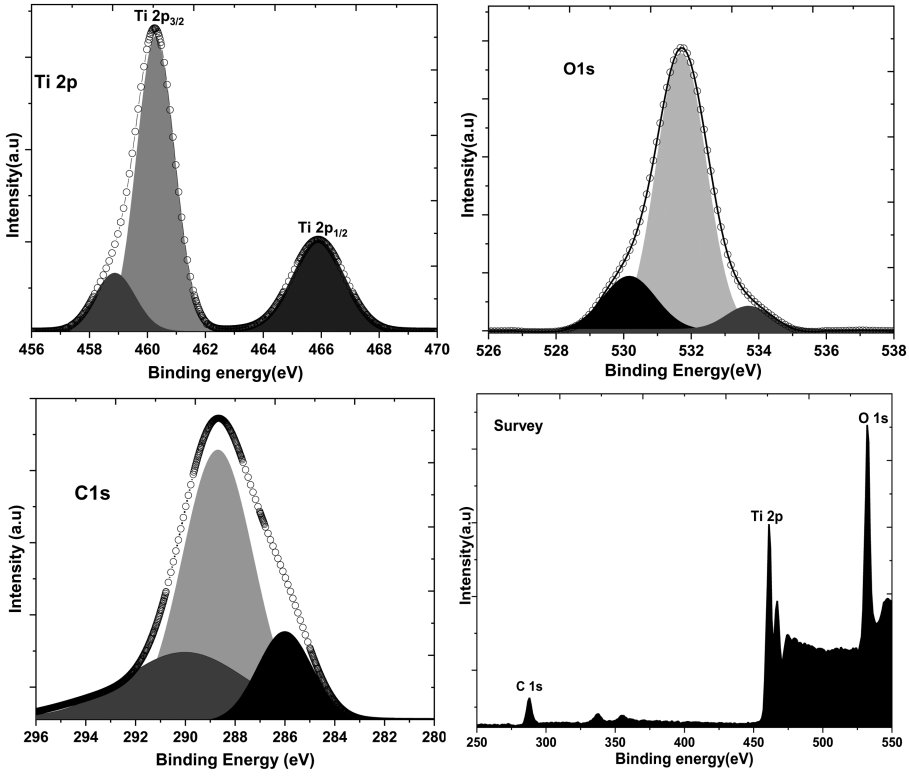

Figure 4. X-ray photoelectron spectra of TiO_2 nanoparticles.

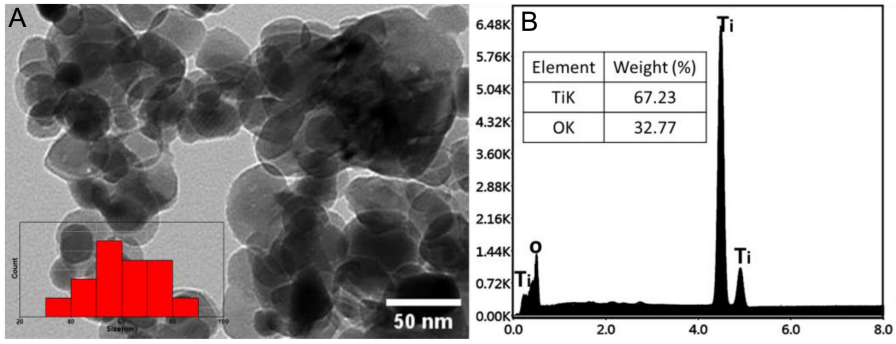

Figure 5. (A) Transmission electron microscopy image (inset), particle size, and (B) Energy-dispersive X-ray spectroscopy (EDS) graph of TiO_2 nanoparticles.

the calculated band gap of the TiO_2 nanoparticles, determined to be 3.2 eV. This band gap aligns with the value reported for TiO_2 anatase.[30]

The FTIR spectrum provides essential information about the organic molecules that envelop the surfaces of nanoparticles. Vibrations at a wavenumber of 3151 cm^{-1} (refer to Figure 3B) confirm the presence of OH groups on the TiO_2 nanoparticles. Furthermore, the vibration at 521 cm^{-1} indicates the Ti-O group vibration.[31]

Peaks at positions 134, 384, 504, and 628 cm^{-1}, corresponding to Eg, B1g, A1g/B1g, and A1g modes, respectively, are indicated by the Raman results of TiO_2 nanoparticles (Figure 3C). These modes align with typical TiO_2 anatase modes as reported in previous studies on TiO_2 nanoparticles.[17] Distinctive peaks associated with anatase titanium dioxide are observable in the XRD pattern of the synthesized TiO_2 nanoparticles (refer to Figure 3D). The anatase phase of titania is identified by its characteristic peaks located at 25.3°, 37.8°, 48.1°, 54.0°, 55.0°, 62.7°, and 68.8° (JCPDS #21-1272).

The XPS analysis conducted on the TiO_2 nanoparticles uncovers the presence of titanium (Ti) and oxygen (O) elements, along with indications of air contamination (refer to Figure 4). Within the Ti2p spectrum, 2 prominent peaks emerge at 458.4 eV and 464.0 eV, corresponding to $Ti2p_{3/2}$ and $Ti2p_{1/2}$, respectively. These peak positions align with the reported binding energies for Ti in TiO_2, affirming that the Ti within the TiO_2 nanoparticles exists in both +4 and +2 oxidation states.[17,32,33] A distinct peak at approximately 530 eV is observed within the O1s spectrum of the TiO_2 nanoparticles, precisely aligning with the characteristic binding energy of oxygen in TiO_2.[34] A peak is detected at 284.6 eV in the C1s spectrum, corresponding to the binding energy of carbon typically found in hydrocarbons. This observed peak is likely attributed to surface contamination resulting from exposure to air.[35]

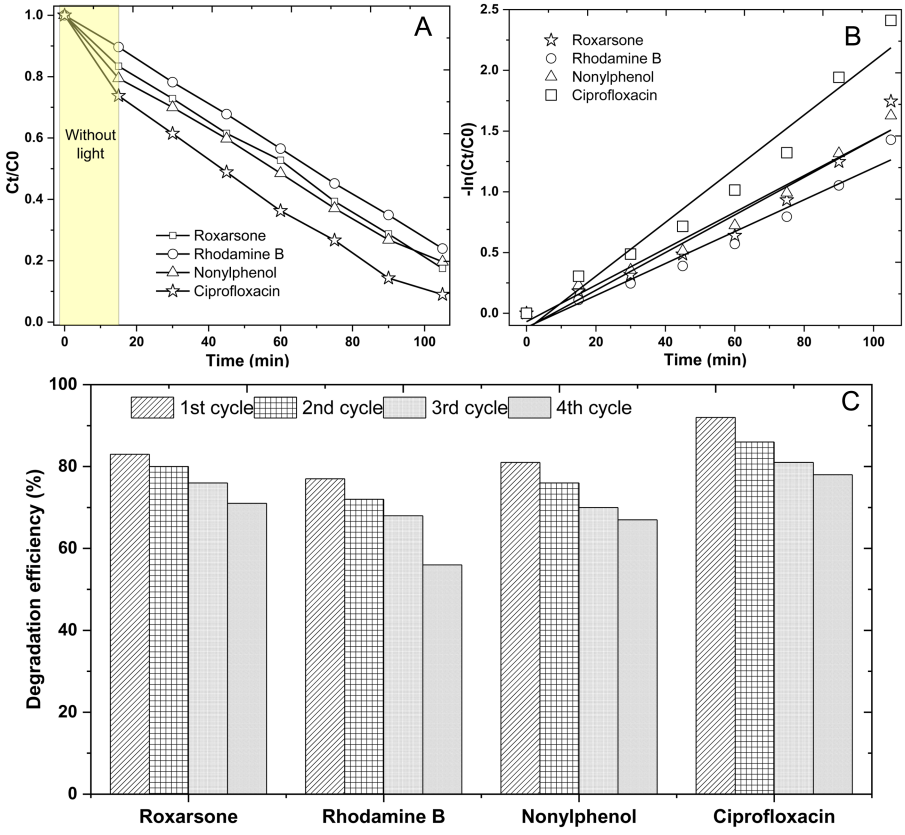

Figure 6. A) Roxarsone, B) Rhodamine B, C) Ciprofloxacin and D) Nonylphenol degradation efficiency using TiO_2 nanoparticles.

The spherical shape of the TiO_2 nanoparticles, with a size of ≥80 nm (depicted in the inset of Figure 5A), is evident in the TEM image (Figure 5A). Additionally, the TiO_2 nanoparticles exhibit high purity, as confirmed by the presence of both titanium (Ti) and oxygen (O) elements (Figure 5B). Specifically, the nanoparticle composition comprises 67.23% titanium (Ti) and 32.77% oxygen (O).

PHOTOCATALYTIC EFFICIENCY

After 105 minutes, the UV absorbance readings demonstrate degradation efficiencies of 83% for roxarsone, 77% for rhodamine B, 81% for nonylphenol, and 92% for ciprofloxacin (refer to Figure 6A). To calculate the kinetic rate constant using equation 2, a pseudo-first-order kinetic equation was applied to quantify these degradation rates. Utilizing this mathematical approach offers a comprehensive insight into degradation kinetics, emphasizing the dynamics of the reaction over time.[36,37]

$$-\ln\frac{\mathbf{Conc._0}}{\mathbf{Conc._t}} = k_t \qquad (2)$$

Upon examining the linear logarithmic plot against irradiation time, it becomes apparent that the photodegradation reaction closely adheres to first-order kinetics, displaying an almost linear pattern. In this study, the rate constants (*k*) for this reaction have been calculated as 0.012, 0.011, 0.015, and 0.02 min^{-1} for roxarsone, rhodamine B, nonylphenol, and ciprofloxacin, respectively. Figure 5B effectively illustrates the remarkable photocatalytic efficacy of TiO_2 nanoparticles based on the derived "*k*" values.

The particles were reused for 4 cycles of treatment. Following each treatment, the particles were collected and subjected to multiple washes with distilled water and ethanol. As depicted in Figure 6C, the photocatalytic degradation of pollutants after the fourth cycle treatment shows no significant change, confirming the stability of the particles.

This study successfully demonstrated a single-step sol–gel synthesis of TiO_2 nanoparticles. The photocatalytic experiments underscored the effectiveness of TiO_2 nanoparticles in removing several pollutants under UV light. Notably, remarkable degradation efficiencies ranging from 77% to 92% were achieved for rhodamine B, nonylphenol, roxarsone, and ciprofloxacin after 105 minutes of irradiation. Spectroscopic and microscopic analyses unveiled the nanoparticles' anatase structure and uniform distribution, indicating their promising suitability for practical applications. This study makes a significant contribution to advancing environmentally friendly technologies and practices by effectively addressing the challenge of eliminating these persistent pollutants.

Peer-review: Externally peer-reviewed.

Author Contributions: Concept – I.A., A.R.M.W., H.M., A.B.I.A., M.N.I.O.; Supervision – I.A., A.R.M.W., H.M., A.B.I.A., M.N.I.O.; Resources – I.A., A.R.M.W., H.M., A.B.I.A., M.N.I.O.; Materials – I.A., A.R.M.W., H.M., A.B.I.A., M.N.I.O.; Data Collection and/or Processing – I.A., A.R.M.W., H.M., A.B.I.A., M.N.I.O.; Analysis and/or Interpretation – I.A., A.R.M.W., H.M., A.B.I.A., M.N.I.O.; Writing Manuscript – I.A., A.R.M.W., H.M., A.B.I.A., M.N.I.O.; Critical Review – I.A., A.R.M.W., H.M., A.B.I.A., M.N.I.O.

Acknowledgments: We are grateful for the assistance provided by the National Forensic Sciences University.

Declaration of Interests: The authors declare that they have no competing interests.

Funding: The authors declared that this study has received no financial support.

REFERENCES

1. Danner MC, Robertson A, Behrends V, Reiss J. Antibiotic pollution in surface fresh waters: occurrence and effects. *Sci Total Environ*. 2019;664:793-804. [CrossRef]
2. Balarabe BY, Bowmik S, Ghosh A, Maity P. Photocatalytic dye degradation by magnetic XFe2O3 (X: Co, Zn, Cr, Sr, Ni, Cu, Ba, Bi, and Mn) nanocomposites under visible light: a cost efficiency comparison. *J Magn Magn Mater*. 2022;562:169823. [CrossRef]
3. Yaou Balarabe B, Illiassou Oumarou MN, Koroney AS, Adjama I, Ibrahim Baraze AR. Photo-oxidation of organic dye by Fe2O3 nanoparticles: catalyst, electron acceptor, and polyurethane membrane (PU-Fe2O3) effects. *J Nanotechnol*. 2023;2023:1-12. [CrossRef]
4. Balarabe BY, Maity P, Teixeira ACSC, Iwarere SA. h-BN nanosheet-modified Ag2WO4 nanocomposite for improved photocatalytic dye removal: insights into catalyst stability and reusability. *Inorg Chem Commun*. 2023;158. [CrossRef]
5. Dzinun H, Othman MHD, Ismail AF, Puteh MH, Rahman MA, Jaafar J. Photocatalytic degradation of nonylphenol by immobilized TiO2 in dual layer hollow fibre membranes. *Chem Eng J*. 2015;269:255-261. [CrossRef]
6. Balarabe BY, Irédon A, Hassimi M, Illiassou Oumarou MN, Masiyambiri V, Gunda TJ. Effective removal of emerging organic pollutants using hybrid Ag@ZnO supported reduced-graphene oxide nanocomposite under visible light. *Hybrid Advances*. 2023;100114. [CrossRef]
7. Hu X, Hu X, Peng Q, et al. Mechanisms underlying the photocatalytic degradation pathway of ciprofloxacin with heterogeneous TiO2. *Chem Eng J*. 2020;380. [CrossRef]
8. Yaou Balarabe B, Paria S, Sekou Keita D, et al. Enhanced UV-light active α-Bi2O3 nanoparticles for the removal of methyl orange and ciprofloxacin. *Inorg Chem Commun*. 2022;146:110204. [CrossRef]
9. Masiyambiri V, Yaou Balarabe B, Adjama I, Moussa H, Illiassou Oumarou MN, Iro Sodo AM. A study of the phytoremediation process using water lettuce (Pistia Stratiotes) in the removal of ciprofloxacin. *Am J Life Sci Innov*. 2023;1(3):1-8. [CrossRef]
10. Jackson BP, Bertsch PM, Cabrera ML, Camberato JJ, Seaman JC, Wood CW. Trace element speciation in poultry litter. *J Environ Qual*. 2003;32(2):535-540. [CrossRef]
11. Bednar AJ, Garbarino JR, Ferrer I, et al. Photodegradation of roxarsone in poultry litter leachates. *Sci Total Environ*. 2003;302(1-3):237-245. [CrossRef]
12. Makris KC, Quazi S, Punamiya P, Sarkar D, Datta R. Fate of arsenic in swine waste from concentrated animal feeding operations. *J Environ Qual*. 2008;37(4):1626-1633. [CrossRef]
13. Liu X, Zhang W, Hu Y, Cheng H. Extraction and detection of organoarsenic feed additives and common arsenic species in environmental matrices by HPLC–ICP-MS. *Microchem J*. 2013;108:38-45. [CrossRef]
14. Olsen CE, Liguori AE, Zong Y, Lantz RC, Burgess JL, Boitano S. Arsenic upregulates MMP-9 and inhibits wound repair in human airway epithelial cells. *Am J Physiol Lung Cell Mol Physiol*. 2008;295(2):L293-L302. [CrossRef]
15. Stolz JF, Perera E, Kilonzo B, et al. Biotransformation of 3-nitro-4-hydroxybenzene arsonic acid (Roxarsone) and release of inorganic arsenic by clostridium species. *Environ Sci Technol*. 2007;41(3):818-823.
16. D'Angelo E, Zeigler G, Beck EG, Grove J, Sikora F. Arsenic species in broiler (Gallus gallus domesticus) litter, soils, maize (Zea mays L.), and groundwater from litter-amended fields. *Sci Total Environ*. 2012;438:286-292. [CrossRef]
17. Balarabe BY, Maity P. Visible light-driven complete photocatalytic oxidation of organic dye by plasmonic Au-TiO2 nanocatalyst under

batch and continuous flow condition. *Colloids Surf A Physicochem Eng Asp*. 2022;655:130247. [CrossRef]
18. Rauf MA, Meetani MA, Hisaindee S. An overview on the photocatalytic degradation of azo dyes in the presence of TiO2 doped with selective transition metals. *Desalination*. 2011;276(1-3):13-27. [CrossRef]
19. Emadian SS, Ghorbani M, Bakeri G. Magnetically separable CoFe2O4/ZrO2 nanocomposite for the photocatalytic reduction of hexavalent chromium under visible light irradiation. *Synth Met*. 2020;267:116470.
20. Gil A, García AM, Fernández M, et al. Effect of dopants on the structure of titanium oxide used as a photocatalyst for the removal of emergent contaminants. *J Ind Eng Chem*. 2017;53:183-191. [CrossRef]
21. Ohtani B, Prieto-Mahaney OO, Li D, Abe R. What is Degussa (Evonik) P25? Crystalline composition analysis, reconstruction from isolated pure particles and photocatalytic activity test. *J Photochem Photobiol A*. 2010;216(2-3):179-182.
22. Ohtani B. Preparing articles on photocatalysis - beyond the illusions, misconceptions, and speculation. *Chem Lett*. 2008;37(3):216-229. [CrossRef]
23. Crnjak Orel Z. *MICROWAVE-ASSISTED NON-AQUEOUS SYNTHESIS OF ZnO NANOPARTICLES SINTEZA NANODELCEV ZnO V NEVODNEM MEDIJU POD VPLIVOM MIKROVALOV*.
24. Shankar R, Groven L, Amert A, Whites KW, Kellar JJ. Non-aqueous synthesis of silver nanoparticles using tin acetate as a reducing agent for the conductive ink formulation in printed electronics. *J Mater Chem*. 2011;21(29):10871-10877. [CrossRef]
25. Lamiel C, Nguyen VH, Tuma D, Shim JJ. Non-aqueous synthesis of ultrasmall NiO nanoparticle-intercalated graphene composite as active electrode material for supercapacitors. *Mater Res Bull*. 2016;83:275-283. [CrossRef]
26. Marycleopha M, Balarabe BY, Adjama I, Hassimi M, Anandaram H, Razak MWA. Anhydrous sol-gel synthesis of anatase TiO2 nanoparticles: evaluating their impact on protein interactions in biological systems. *J Trace Elem Med*. 2023:100114. [CrossRef]
27. Atchudan R, Edison TNJI, Perumal S, Karthikeyan D, Lee YR. Facile synthesis of zinc oxide nanoparticles decorated graphene oxide composite via simple solvothermal route and their photocatalytic activity on methylene blue degradation. *J Photochem Photobiol B*. 2016;162:500-510. [CrossRef]
28. Feng Y, Feng N, Wei Y, Zhang G. An in situ gelatin-assisted hydrothermal synthesis of ZnO-reduced graphene oxide composites with enhanced photocatalytic performance under ultraviolet and visible light. *RSC Adv*. 2014;4(16):7933-7943. [CrossRef]
29. Karimipour M, Sadeghian M, Molaei M. Fabrication of white light LED photocatalyst ZnO–rGO heteronanosheet hybrid materials. *J Mater Sci Mater Electron*. 2018;29(16):13782-13793. [CrossRef]
30. Bamola P, Sharma M, Dwivedi C, et al. Interfacial interaction of plasmonic nanoparticles (Ag, Au) decorated floweret TiO2 nanorod hybrids for enhanced visible light driven photocatalytic activity. *Mater Sci Eng B*. 2021;273:115403. [CrossRef]
31. León A, Reuquen P, Garín C, et al. FTIR and Raman characterization of TiO2 nanoparticles coated with polyethylene glycol as carrier for 2-methoxyestradiol. *Appl Sci*. 2017;7(1). [CrossRef]
32. Yaou Balarabe B, Maity P. A polymer-Au/TiO2 nano-composite based floating catalyst for photocatalytic dye degradation under natural sunlight. *J Photochem Photobiol A*. 2024;449:115405. [CrossRef]
33. Yaou Balarabe B. B. Green synthesis of gold-titania nanoparticles for sustainable ciprofloxacin removal and phytotoxicity evaluation on aquatic plant growth. *Hybrid Adv*. 2023;4:100107. [CrossRef]
34. Mezni A, Ibrahim MM, El-Kemary M, et al. Cathodically activated Au/TiO2 nanocomposite synthesized by a new facile solvothermal method: an efficient electrocatalyst with Pt-like activity for hydrogen generation. *Electrochim Acta*. 2018;290:404-418. [CrossRef]
35. Mao J, Zhao B, Zhou J, et al. Identification and characteristics of catalytic quad-functions on Au/anatase TiO2. *ACS Catal*. 2019;9(9):7900-7911. [CrossRef]
36. Potle VD, Shirsath SR, Bhanvase BA, Saharan VK. Sonochemical preparation of ternary rGO-ZnO-TiO2 nanocomposite photocatalyst for efficient degradation of crystal violet dye. *Optik*. 2020;208. [CrossRef]
37. Di X, Guo F, Zhu Z, Xu Z, Qian Z, Zhang Q. In situ synthesis of ZnO-GO/CGH composites for visible light photocatalytic degradation of methylene blue. *RSC Adv*. 2019;9(70):41209-41217. [CrossRef]